Self-Assembled Biohybrid: A Living Material To Bridge the Functions between Electronics and Multilevel Biological Modules/Systems

Abstract

Exoelectrogens are known to be specialized in reducing various extracellular electron acceptors to form conductive nanomaterials that are integrated with their cell bodies both structurally and functionally. Utilizing this unique capacity, we created a strategy toward the design and fabrication of biohybrid electronic material by exploiting bio-reduced graphene oxide (B-rGO) as the structural and functional linker to facilitate the interaction between the exoelectrogen community and external electronics. The metabolic functions of exoelectrogen encoded in this living hybrid can therefore be effectively translated toward corresponding microbial fuel cell applications. Furthermore, this material can serve as a fundamental building block to be integrated with other microorganisms for constructing various electronic components. Toward a broad impact of this biohybridization strategy, photosynthetic organelles and cells were explored to replace exoelectrogens as the active bioreducing components, and as formed materials exhibited 4- and 8-fold improvements in photocurrent intensities as compared with native bio-electrode interface. Overall, a biologically driven strategy for the fabrication and assembly of electronic materials is demonstrated, which provides a unique opportunity to precisely probe and modulate desired biofunctions through deterministic electronic inputs/outputs and revolutionize the design and manufacturing of next-generation (bio)electronics.

1. Introduction

From biomineralization to microbial symbiosis, living systems are specialized in assembling various levels of components toward biohybrid materials with hierarchical structures and coherent functions such as bones and microbial consortia. Modulating such a biohybridization process provides extensive opportunities in creating materials with integrated bio-bio and bio-abio functions that do not exist in separated systems.^{1–3} Utilizing this unique property, various living materials have been developed, which have demonstrated unprecedented capacities in many applications including sensing,⁴ actuation,⁵ and material synthesis.⁶ Incorporation of emerging tools such as genetic editing,^{1,7–9} and bioprinting^{10–12} offer possibility in precise modulation of the structures and functionalities, which further extend the potential implementation of living components beyond existing territories to revolutionize how we design and synthesize functional materials.^{2,13,14}

Among all organisms that have been exploited in the synthesis of biohybrid living materials, exoelectrogens such as Shewanella loihica PV-4 (PV-4) and Geobacter sulfurreducens DL-1 are known for their unique capability to electrically interact with extracellular electron acceptors and in situ deposit inorganic nanomaterials such as Ag, Au, Pd and FeSx nanoparticles on their outer membranes.^{15–17} In addition to structural consolidation, these nanomaterials were also intrinsically wired with the bacteria's metabolic electron transfer pathway. 18,19 As the most significant functions of exoelectrogens such as synthesis, sensing, and information-processing are dominated by their metabolic electron transfer, 20 these nanomaterials were capable of interfacing such exoelectrogens functions with extracellular electronics. 21 Through the electronics enabled precise detection and modulation, this nanomaterial/exoelectrogens hybrid has the potential to serve as a fundamental building block in developing various bioelectronics (e.g., biosensors, microbial fuel cells, etc.).22-24 Previously, we have exploited graphene oxide (GO) as a terminal electron acceptor, which can be intimated linked with PV-4 in the form of biologically reduced graphene oxide (B-rGO) via extracellular electron transfer. ^{25,26} In contrast with doped nanomaterials, the BrGO is closely coupled with the redox-active sites of the biomachinaries through the active bioreduction process and processes a two-dimensional, honeycomb lattice structure at the microscale, which offers unique advantages to host multiple PV-4 cells to construct an integrated network. Together with interactions such as hydrophobic and electrostatic forces, this B-rGO/EAB matrix can self-assemble to form a free-standing 3-D living material with unique electrical/electrochemical activities.²⁷

Here, we exploited this PV-4/B-rGO biohybrid as a unique material platform for creating various living electronic components from the bottom up. First, the self-assembling process was rationally modulated to encode this living material with desirable mechanical integrity, optimal mass/electron transport, and tunable morphology. A "plug-and-play" microbial fuel cell was made based on the B-rGO wired/interfaced PV-4's extracellular electron transfer. We further expand the device functionality through the cross-species assembly of other microorganisms and built biosynthesized supercapacitors and photosensitive electrodes. Finally, the strategy has been applied to other biologically significant charge transport processes. By integrating photosynthetic

organelles and cells as the living components, we demonstrate the possibility of effectively interpreting photosynthesis with external electrical circuits. We expect that this hybridization strategy will open up new opportunities for many cross-disciplinary applications in biosensing, energy transduction, and hybrid information processing.

2. Results and Discussions

2.1 Synthesis of the PV-4/B-rGO Biohybrid

The PV-4/B-rGO biohybrid was synthesized by culturing precursor solutions composed of PV-4 and graphene oxide (GO) mixing with the desired ratio under an anaerobic condition. Serving as the only terminal electron acceptors, GO was reduced by the metabolic electron of PV-4 and intimately connected with the outer membranes of PV-4. Due to the partial removal of the hydroxyl- and carbonyl- groups decorated on the GO sheets, the B-rGO held increased hydrophobicity together with reduced surface charge density. ^{28–30} This transformation in surface properties introduced hydrophobic attraction while mitigated electrostatic repulsion at both B-rGO/PV-4 and B-rGO/B-rGO interfaces and eventually drove the self-assembly of PV-4 and B-rGO. ³¹ Consequently, the free-standing PV-4/B-rGO biohybrid with a size around 50% smaller than the original PV4/GO precursor solution was synthesized after a 48 hours culture. (Fig. 1a) High magnification SEM images also confirmed the intimate contacts between PV-4 and B-rGO after assembly. (Fig. 1b) It is worth noting that the volume ratio of PV-4 and GO in the precursor solution has to be precisely controlled (5:1 is optimal) to initiate this self-assembling process. Instead of free-standing PV-4/B-rGO biohybrid, small PV-4/B-rGO agglomerations would be obtained if the ratio was altered.

Based on our observation, the 3-D profile of the PV-4/B-rGO biohybrid was determined by both (i) the boundaries of the culture container (in x-y axis) and (ii) the height of the precursor solution (z-axis). Therefore, a molding method was developed to achieve morphological controls of the biohybrid during self-assembling through tuning these two parameters. As presented in Fig. 1c, biohybrids with various shapes such as disc, pillar array, and wires could be synthesized by using cultural containers with corresponding shapes. Furthermore, the thickness of the biohybrids can be tuned from 0.3 to 3 mm by controlling the height of precursor solution; whereas the selfassembly of PV-4 and B-rGO was prohibited when solution height is below 0.3 mm. This phenomenon may be attributed to the effect of oxygen diffusion into the thin solution layer as oxygen can serve as a soluble electron acceptor to restrict the reduction of GO.32 Overall, this molding method enables design flexibility in this biofabrication strategy, which was expected to implementation of various electronic modules facilitate the with controlled microstructure/dimensionality (such as 1D, 2D, and 3D electrodes).

This biohybrid can host PV-4 at a density of $6.4x10^9$ cells/cm³, which is one to two orders of magnitudes higher than native biofilms (estimated based on original cell density in precursor solution and a 25 µm thickness of native biofilm). In addition, the high metabolic rate of PV-4 can be sustained through this biohybrid by the conductive B-rGO, in contrast to native biofilms where exoelectrogens exhibit low metabolic activity due to the intrinsic charge transport limit. Although varying the composition can alter the conductivity, (Fig. S1) the PV-4/B-rGO biohybrid held a conductivity up to 129 µS/mm at the completion of self-assembling (Fig. 1d), which is superior to most reported native exoelectrogen biofilms to the best of our knowledge. S5-37 Besides, our previous research has suggested that the B-rGO can promote the functional integration

between exoelectrogen and external electronics by significantly reducing the charge transport barrier at the bio-electronic interface.²⁶ Combining the high load of PV-4, efficient charge transport (i.e., conductivity), and minimized bio-electronic barrier, this biohybrid was capable of effectively bridging the biofunctions of PV-4 to construct high-performance living electronics.

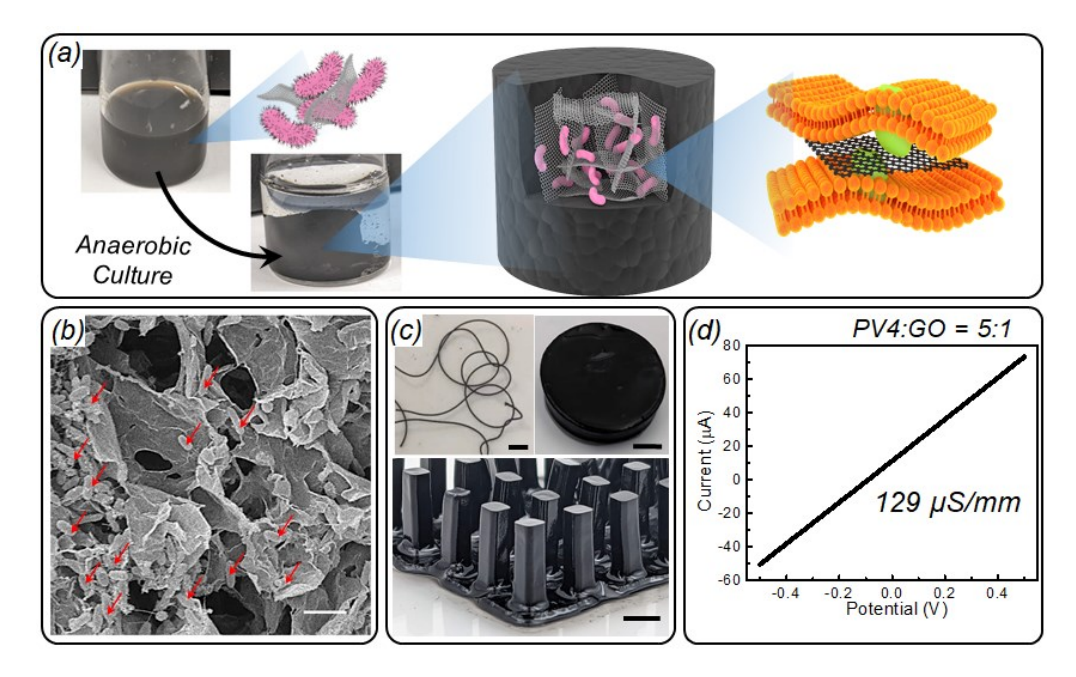


Figure 1. PV-4/B-rGO biohybrids - (a) Schematic illustrations of the synthesis process of the PV-4/B-rGO biohybrid. (b) SEM images of the PV-4/B-rGO biohybrid, of which the red arrows indicated PV-4 which are intimately integrated into the 3-D B-rGO matrix. (Scale bar: $2 \mu m$) (c) Biohybrids with various 3-D profiles (Wire (Scale bar: 2 mm); Disc (Scale bar: 5 mm) and pillar array (Scale bar: 5 mm)) synthesized by the "molding" methods. And (d) Two probe electrical measurement of biohybrid made of a 5:1 (PV-4: GO) precursor solution. This biohybrid holds the highest conductivity at $129 \mu S/mm$ among all synthesis conditions.

2.2 PV-4 based Living Electronics

Toward designing living electronics, biological functions of the PV-4/B-rGO biohybrid were characterized through a series of cyclic voltammetry (CV) measurements. Particularly, the biohybrid was connected with an electrochemical working station by a titanium wire immediately after self-assembly to serve as the working electrode. Platinum and Ag/AgCl were used as the counter- and the reference- electrodes, respectively. As shown in Fig. 2a, a distinguished reduction peak at around -0.2 V as well as a broad oxidation peak at 0.1 V can be observed on the CV profile of biohybrid when the applied scan rate is at 10 mV/s. These redox peaks corresponded to the single electron Fe^{III}/Fe^{II} redox reaction at the heme center of outer membrane cytochromes (OMCs) of PV-4,³⁸ which suggested that the metabolic electron transfer was seamlessly linked with the conductive matrix. In addition, the reduction peaks shifted to a more negative potential along with increasing the CV scan rate while the peak current varies linearly, consistent with the behavior of a quasi-reversible system. (Fig. S2a and b) ³⁹ Besides, the oxidation peak vanished at a fast CV scan rate (Fig. S2a). Both results further confirmed that charge transport in the biohybrid was dominated by the OMCs that held intermediate charge transport rate; hence charges accumulated at the cytochromes when a fast scan rate was applied.

The CV measurements also demonstrated a unique advantage of the PV-4/B-rGO biohybrid. In contrast to conventional exoelectrogen-based electronics (i.e., microbial fuel cells (MFC)) that required a long start-up period (hours to days) before operation, 40,41 this biohybrid established bioelectrochemical equilibrium shortly after synthesis. This "plug-and-play" feature enabled this biohybrid to serve as a versatile module for developing various living electronics with improved agility and reusability. As a proof of concept, a free-standing MFC was developed by connecting this biohybrid with stainless steel electrodes directly (Fig. 2b insert). As shown in the results (Fig. 2b), this MFC generated currents immediately after the electrodes connected with biohybrids ("On", the yellow regions) with the magnitude in a µA range that was commonly obtained in many existing MFCs. 42 Furthermore, this generated current vanished after the biohybrid was disconnected ("Off", the gray regions). Through repeating this connectiondisconnection cycle, the start-up time of this MFC is measured at hundreds of seconds range, which was comparable with most "fast response" MFC that required sophisticated microfabrication to accelerate their response (e.g. by reducing device volumes). 23,43,44 Overall, this biohybrid MFC featured with zero start-up period, sufficient efficiency, and fast response time was expected to bring in new insight into the design and application of exoelectrogen-based bioelectronics to explore their optimal performance and functionality in energy generation, sensing, and electrocatalysis.

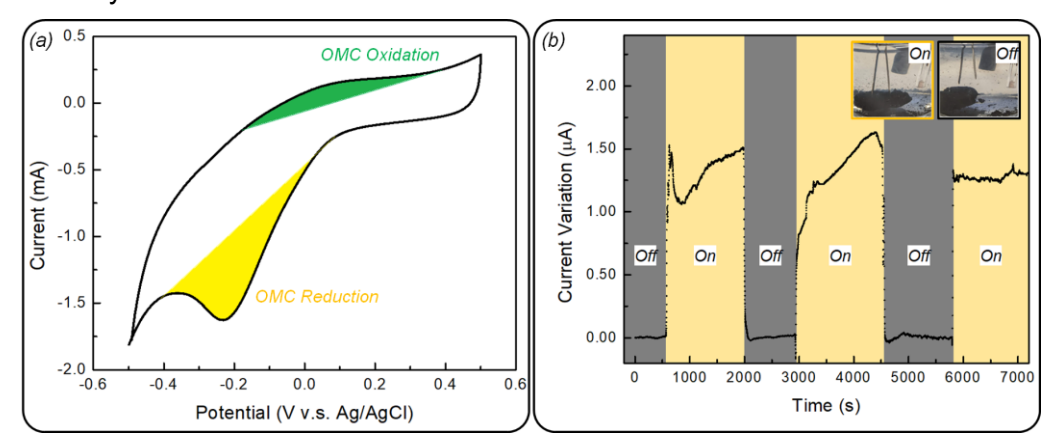


Figure 2. Electrochemical properties of the PV-4/B-rGO biohybrids- (a) CV measurements at 10mV/s scan rate. The Fe^{III}/Fe^{II} redox reaction PV-4's OMCs can be clearly observed in the CV scan. (b) the current-time (I/T) measurements of the plug-and-play MFC, of which the PV-4/B-rGO biohybrid was connected with stainless steel working electrode during the "On" period (yellow) while disconnected during the "Off" period. The insert images presented the repeatable connection/disconnection between the biohybrid and the working electrode.

2.3 Supercapacitor: Biohybrid Enabled Cross-Species, Structural Integration

In nature, many microorganisms were capable of living and growing symbiotically to construct a microbial consortium with integrated structure and function. Based on such capacity, we "grew" a supercapacitor from the bottom-up through modulating the development of microbial consortium to simulate the conventional fabrication process in the electronic industry. The fabrication process was detailed in the material and method part. In short, the bacterial cellulose (BC) layer was first synthesized using G. *xylinus*. Next, GO solution was adsorbed on both sides of BC followed by a two-day PV-4 culture forming an integrated G. *xylinus*/B-rGO/PV-4 consortium, (Fig 3a middle). Consequently, this consortium was transformed into a supercapacitor by a series of glutaraldehyde fixing, drying, and trimming processes (Fig 3a bottom), of which, the intimate

contact between BC and PV4/B-rGO were observed using SEM (Fig. 3b). The Randles circuit fitting of an electrochemical impedance spectroscopy measurement showed a low charge-transfer resistance (3.7 Ω) at the interface between BC and PV4/B-rGO, which suggested that this process would not damage both structural- and functional- integrities of this supercapacitor. (Fig. 3c)

In this supercapacitor, the insulated BC acted as a separator/electrolyte layer while the PV-4/B-rGO performed as the electrodes, which can store charges through (1) electrical double layer capacitance at the electrode/electrolyte interface; and (2) pseudocapacitance attributed to redox activity of PV-4's outer membrane cytochrome. To evaluate the capacitance performance of this self-assembled supercapacitor, cyclic voltammetry (CV) and Galvanostatic charge-discharge measurements (GCD) were conducted with scan rates and current densities varied from 10 to 500 mV/s and 0.02 to 0.3 A/g, respectively. As shown in Fig. 3d, the guasirectangular shape of CV and the triangle shape of GCD imply good capacitive properties. Areal capacitance value at a scan rate of 500 mV/s was calculated as 10 mF/cm², which was similar to many existing thin-film supercapacitors fabricated by the common lamination method. 45,46 Nevertheless, the specific mass capacitance calculated from GCD curves varies from 6.28 F/g to 2.1 F/g over different current densities (detailed in materials and methods) Fig. 3e. The low specific mass capacitance may be ascribed to the larger weight of BC (density = 1.25 g/cm³)⁴⁷ as compared with liquid/gel (density ≈ 1 g/cm³) that is commonly used as an electrolyte layer. Through this research, we demonstrated a novel bio-derived strategy to fabricate complicated electronic devices from the bottom up. Encompassing many unique advantages of biological processes such as low energy consumption, mild condition, and minimized environmental impact, this strategy offered the potential to transform how the electronics were designed and fabricated to ensure the sustainability of the modern electronic industry.

2.4 Photosensitive Electronics: Biohybrid Enabled Cross System, Functional Integration

In the PV-4/B-rGO biohybrid, the outer membrane cytochromes of PV-4 were seamlessly connected with conductive B-rGO as confirmed by previous research in 2.1 and 2.2. Since cytochromes were also ubiquitous redox mediators in various biological systems, ⁴⁸ we suggested that the inherent redox activity and conductivity make this material an excellent bio-electronic interface to enable the electrical access of many biofunctions. To test this hypothesis, thylakoid membrane (TM) was selected as a model system to be integrated with electronics using the PV-4/B-rGO interface. Compared with other higher-level photosynthetic organisms (cyanobacteria, plants), TM doesn't respirate; therefore, interference from other intercorrelated redox signals can be minimized; hence serves as an excellent model for this research. ⁴⁹ The scheme of this photosensitive electronics was presented in Fig. 4a. In this electrode, electrons were first generated on TM as a result of photo-induced water oxidation at an oxygen-evolving complex of the photosystem II complex. Next, this redox-driven electron transfer was effectively transduced by the PV-4/B-rGO interface to be detected by external electronics.

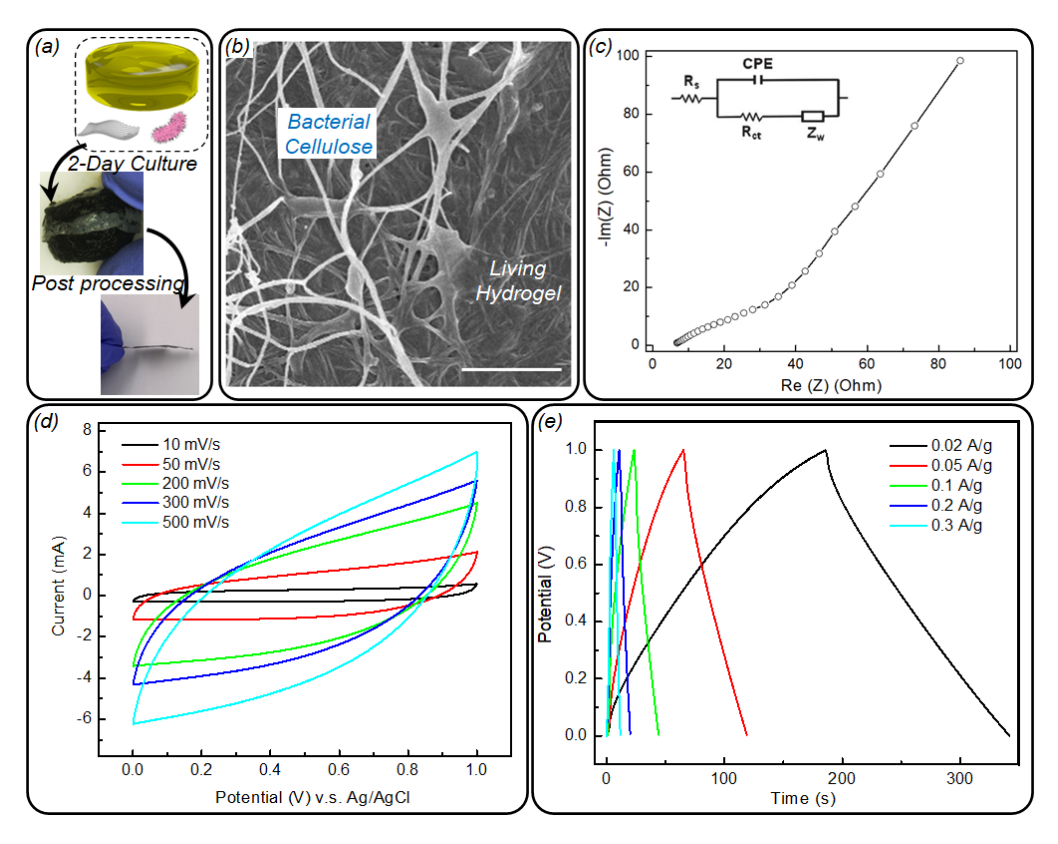


Figure 3. Bio-assembled supercapacitor - (a) schematic and image of the bioderived assembling process. (b) SEM images of the bacterial cellulose/ PV-4/B-rGO biohybrids interface in the assembled supercapacitor. (Scale bar=2 μ m) (c) the electrochemical impedance spectroscopy measurement of the supercapacitor and its equivalent Randles circuit, of which the CPE stands for constant phase element that associated with double layer capacitance, R_s is the solution resistance, Z_w is the Warburg element and R_{ct} is the charge-transfer resistance at the interface between BC and PV4/B-rGO (3.7 Ω). (d) Cyclic voltammetry of the supercapacitor with different scan rates. And (e) GCD curves of the supercapacitor at different current densities.

As presented in the measurement, redox signals originating from the photosynthesis electron transfer can be effectively wired with electronics after simply drop-casting TM on the redox-active PV-4/B-rGO interface (red curve in Fig. 4b). In contrast, the ITO electrode with TM immobilized only demonstrates a low-magnitude photo-responsive current. (black curve in Fig. 4b), further validating the critical role of the biohybrid to transduce the redox signals from TM. We suggested that the success in the cross-system coupling of redox signals can be attributed to two unique properties of the biohybrid: (1) the biohybrid surface is hydrophilic (Fig. S3) and chemically active due to the presence of PV-4. Therefore, this biohybrid can provide a compliant microenvironment to accommodate TM while preserving its functions as previously demonstrated in many hydrogel-based bioelectronics.⁵⁰ And (2) in common electronics, the transduction of biologically derived redox signals has relied on electrochemical reactions that can lead to signal attenuation.⁵¹ On the contrary, redox mediators (i.e., OMC) were intimately coupled with B-rGO,²⁶ thus capable of more effectively transducing external input through correspondent redox pathways. Based on this property, this PV-4/B-rGO biohybrid is expected to contribute to the optimal integration of electronics with the redox signals of various bio-machineries. As redox signaling is involved in many physiological processes such as cell differentiation, proliferation, and immune response,52 this interface will open up many possibilities in developing highperformance bioelectronics such as point-of-care biosensors and high throughput drug screening tools.

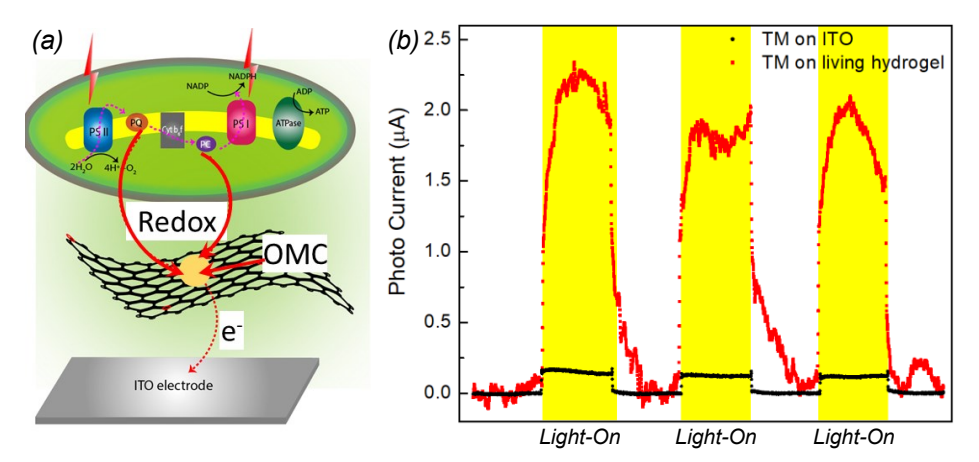


Figure 4. PV-4/B-rGO biohybrids interfaced photo current transducer – (a) Scheme of the biohybrid interfaced photo electron transfer, of which outer membrane cytochromes (OMC) of PV-4 inside the biohybrid can wire the redox molecules driven electron transfer cascades on thylakoid membrane (TM) toward graphene that hold effective electrical connection with remote electronics. Through this functional connection, the biological redox to electrical signals transduction can be effectively conducted. (b) 5-folds enhancement on the magnitudes of detected photo current on device with biohybrid interface (red curve) than ITO electrode/TM contact (Red curve). The results indicated that OMC is of critical in the effective connection/translation of biological redox toward electrical signals.

2.5 Expanded paradigm: Living electronics integration through alternative bioreductive processes

Finally, the possibility of integrating a broader range of bio-machineries within the conductive rGO matrix has also been examined by exploiting different biological electron transfer processes. First, we attempted to directly wire the photosynthesis electron transfer on TM through *in-situ* bioreduction of GO-based on a similar principle of the PV-4/B-rGO self-assembly. Specifically, freshly prepared TM solutions were drop-casted on a GO-coated ITO electrode and then incubated in a 4°C chamber where simulated sunlight was illuminated continuously to trigger a bioreduction process to form the TM/B-rGO film on ITO.

To evaluate the efficiency of the B-rGO induced TM-electronics integration, photocurrent intensity of this TM/B-rGO film was measured by CV (range: -0.5 and 0.5 V vs. Ag/AgCl) and a pure TM film was applied as a control sample. As shown in Fig. 5a, the CV of the TM/B-rGO presented a high-intensity redox couple peaks with mid-potential at -0.1V, which were belonged to the redox activity of the quinone electron acceptors in photo system II of TM as suggested in previous research.⁵³ To validate this assumption, an inhibitor of photo synthesis electron transfer, DCMU (3-(3,4-dichlorophenyl)-1,1-dimethylurea), was applied, which eliminated the formation of redox peaks of the TM/B-rGO film under identical CV measurement conditions. This result confirmed that the redox peaks were originated from TM photosynthesis (Fig. S4). In contrast, attenuated redox couple peaks at similar potentials were observed in the measurement of pure TM film. These measurements implied that the B-rGO can facilitate the direct electron transfer between TM and external electronics.

Toward creating bio-derived photosensitive electronics, amperometric measurements upon light on/off cycles were performed on the TM/B-rGO film, when the potential at 0.5 V vs. Ag/AgCl was constantly applied. As shown in Fig. 5b, the TM/B-rGO presented an eight-time (15to 120- nA) increase in signal (i.e., current) intensity as compared with pure TM film. Besides, agile response to light was observed in the measurement, which may be resonated to the complex electron transfer chain in the TM. As both photosynthetic and respiratory activities commonly coexist in cyanobacterial TM, which share many electron transfer components, respiration can detain photosynthetic electron transfer until the depletion of respiratory electron acceptors; therefore, causing the agile response.^{54,55} Nevertheless, we proposed that whole cells (i.e., cyanobacteria) can self-regulate the photosynthetic- and respiratory- electron transfers due to their comprehensive cellular functions, which minimized this agile photo-current response (Fig. 5c). Altogether, this TM/B-rGO film was expected to serve as both a unique tool to study the electron transfer on TM and a solid fundament to develop high-performance photosensitive electronics. Whereas the progressive increase in current during measurement suggested that the electron transfer rate may still be restricted at the TM-B-rGO interface and further optimization was inevitable. In addition, this biosynthetic strategy was also applied to integrate photosynthetic systems at whole-cell levels. Anabaena, a genus of nitrogen-fixing cyanobacteria, was mixed with GO on ITO under the illumination of simulated sunlight for 12 hrs, Current-time measurements were applied to determine the photo-electrochemical activity of the Anabaena/rGO biohybrid. As illustrated in Fig. 5c, the intensity of photo-induced current was increased by 10-time when Anabaena was hybridized with B-rGO. Overall, these tests of TM and Anabaena demonstrated extensive potential in integrating desired biological functions with electronics through this bioenabled hybridization strategy.

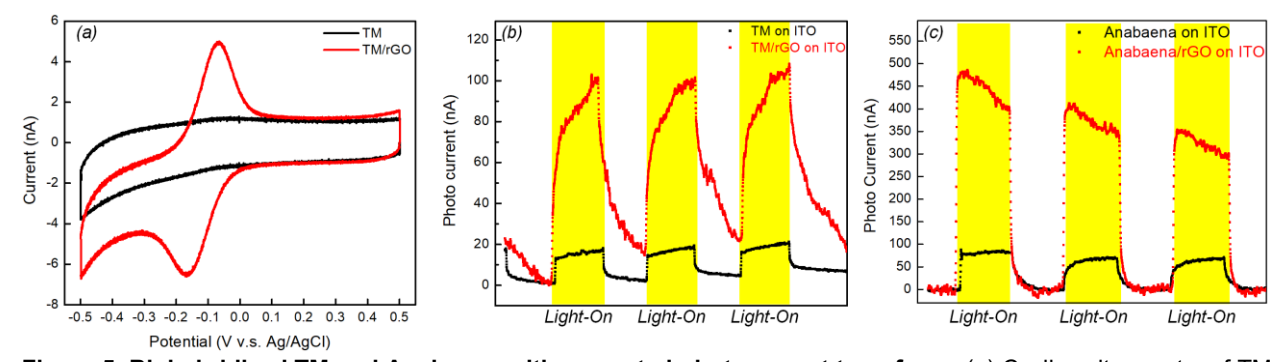


Figure 5. Biohybridized TM and Anabaena with promoted photocurrent transfers – (a) Cyclic voltammetry of TM on bare ITO- and GO coated ITO- electrodes. The results indicated that the GO was *in-situ* reduced to rGO by photosynthesized electron of TM. The synthesized rGO can effectively interface the electron transfer of TM toward external electronics as indicated by the increase intensities of the redox peaks. (b) and (c) Comparisons of the photo currents intensities with/without rGO interfaced TM (b) and *Anabaena* (c). Applied potential was fixed at 0.5 V.

3. Conclusion

In conclusion, we created a structurally- and functionally- coherent biohybrid by harnessing the biomineralization process to assemble the biotic and electronic modules from the bottom-up. In this biohybrid, biological electron transfers are effectively wired to external electronics, which enables electrical access to the encoded biological function in energy generation. Other biological machineries were further integrated on this biohybrid to demonstrate

a possibility in constructing devices with the charge generating and storage functionalities through biologically driven self-assembly. Moreover, this bio-initiated hybridization strategy can be extended to other biological systems for programming the functions of assembled bioelectronics. As a proof of concept, light-sensitive devices were created utilizing thylakoid membrane and cyanobacteria. Moving forward, this work represents a strategically new approach in how we design and fabricate bioelectronics, which is expected to open up many opportunities in biosensing, biocomputing, and wearable electronics to completely transform how biological functions are interpreted and modulated.

4. Method

4.1 Synthesis and characterization of PV-4/B-rGO biohybrid

The culture of *S. loihica* PV-4 was based on documented protocol.⁵⁶ In short, *S. loihica* was cultured from –80 °C glycerol stock and inoculated in 50 mL of Luria–Bertani broth (Sigma-Aldrich L3522) with gentle shaking (100 rpm) in the air for 48 h at 25 °C. After centrifuging at 4000 rpm for 20 min, the isolated bacteria were redispersed in mineral media (MM) containing 30 mM sodium lactate to tune the bacteria concentration to 1.26 x 10¹⁰ cell/ml, the formulation of MM was reported previously.⁵⁶ The *S. loihica* solution was then mixed with GO solution (4mg/mL; Sigma Aldrich 777676) in desired volume ratio and cultured for 48 hours under the anaerobic condition to obtain the PV-4/B-rGO biohybrid. To program the morphology of this biohybrid, a "molding" process was exploited. Specifically, the PV-4/GO solutions were filled into the container with customized 3-D profile prior culture, where the synthesized biohybrid can replicate the 3-D profiles and grow into desired structures.

Morphology of the biohybrid was characterized by scanning electron microscope (SEM) imaging. Samples for SEM imaging were prepared as follows: After DI water rinsing, the samples were dehydrated in a series of ethanol solutions (50, 75, 90, 95, 100% and 100%, 10 min each). Dehydrated samples were then critical point dried (Leica EM CPD300) and sputtered with Pd/Pt alloy. Images were acquired by Zeiss Ultra 55 SEM and JEOL 7900F SEM.

The electrical property of the biohybrid was characterized by a direct current I–V measurement using Biological SP200 Potentiostat. To establish electrical contact, the biohybrid were immobilized onto a pair of gold electrodes (1 mm separation) with gentle pressure applied. The measurements were performed after the samples were rinsed with DI water and 100% ethanol.

4.2 MFC measurement

Measurements of MFC performance were done by using a three-electrode set-up in 50 mL glass vials. Specifically, the working electrode was two stainless steel needles (Sigma-Aldrich Z115606) with PV-4/B-rGO biohybrid connected optionally. The Ag/AgCl and platinum wire were used as reference- and counter- electrodes, respectively. The vial was filled with 40 mL PBS, and during measurements, after the current stabilized, the connection and disconnection between the working electrode and living biohybrid were performed repeatedly while the corresponding current changes were recorded.

4.3 Supercapacitor fabrication and measurement

To fabricate the bio-assembled supercapacitor, the bacterial cellulose (BC) based separator was first synthesized by culturing Gram-negative bacteria - *Gluconacetobacter xylinus* (https://www.atcc.org/products/53582) in a static condition until pellicle formed in a six-well plate. Then BC pellicle was transferred into a new 6 well plate for assembly of the PV4/B-rGO electrodes. First, GO solution was soaked on both sides of the BC pellicle for 12 hours to decorate GO on both surfaces of the BC pellicle. Following this, PV-4 cultural solution was added to one side of the GO-decorated BC pellicle and incubated at room temperature to initiate bacteria-driven GO reduction. After 24-hour, the BC pellicle was flipped and repeated adding 1 mL bacteria on the other side to finally obtain the bio-assembled supercapacitor.

The performance of the supercapacitor was evaluated using cyclic voltammetry (CV), galvanostatic charge-discharge (GCD) cycles, and electrochemical impedance spectroscopy (EIS). A Bio-Logic SP-200 Potentiostat with EC-Lab software (Biologic) was used for all electrochemical techniques. In all measurements, carbon cloth and Ag/AgCl were applied as a counter electrode and a reference electrode, respectively. The CV was obtained under a three-electrode configuration with a potential range of 0 to 1.0 V and the scan rate varied from 10 to 500 mV/s. GCD was performed in a two-electrode setup with a range from 0.02 A/g to 0.3 A/g. The specific capacitances (C_s) of electrodes derived from galvanostatic discharge curves were calculated by using the equation:

$$C_S = \frac{2I}{m\frac{\Delta V}{\Lambda t}},$$

where I is the constant discharge current, m is the mass of one electrode and ΔV and Δt represent voltage change (excluding V_{drop}) on discharge and time for full discharge respectively. Besides, the EIS was performed with a frequency range between 100 kHz and 0.1 kHz and an AC perturbation of 10 mV.

4.4 Photoelectrochemical measurements

4.4.1 Isolation of TM from Spinach Leaves

Selected 40 g of dark green leaves and rinsed leaves in cold water. Grinded leaves in about 150–175 mL of Buffer A (Table S1) and filtered the homogenate twice on two layers of cloth tissue. Collected the filtrate and centrifuge at 750 × g for 15 min. Discarded the supernatant and resuspended the pellet in about 30 mL of Buffer B. Centrifuged the filtrate 60 s at 750 × g and resuspend the pellet in a small volume of Buffer B (1–1.5 mL). The total chlorophyll concentration of the chloroplast preparation is measured according to below protocol:

- a. Added 10 mL of chloroplast preparation in 5 mL of 80% acetone and vortex the mixture.
- b. Centrifuged the mixture for 2 min at 2,500 × g.
- c. Carefully transfer the supernatant in the spectrophotometer cuvette.
- d. Measured the absorbance of the supernatant at 647 and 664 nm using the spectrophotometer.
- e. Calculated the chlorophyll concentration using the following equation: Chlorophyll concentration (mg/mL) = $[(17.76 \times A647) + (7.34 \times A664)]/2$

The final TM concentration in this preparation was around 1 mg/mL.

4.4.2 Anabaena culture

Anabaena sp. was bought from Carolina Biological. To set up a new culture (a subculture), transferred about 10 mL of a stock culture into 200 mL of fresh medium (Alga-Gro®). The detailed components are shown in Table S2. Placed the new culture under cool-white, fluorescent lights (200 to 400 foot-candles) for 7 to 10 days to allow the alga to grow. Once there was good growth, moved the culture to an area of lower illumination (50 to 100 foot-candles) for slower growth and storage.

4.4.3 Preparation of modified electrodes

ITO substrates with 25 mm \times 25 mm rectangular shape were cleaned in an ethanol solution and sonicated for 30 min, then rinsed with deionized water and dried with N₂. Prior to experiments, these ITO substrates were treated by oxygen plasma at 100 W for 60 s (Plasma-Etch PE-50 XL benchtop plasma cleaner) to increase their hydrophilicity. Self-made a small chamber by cutting 15 mL centrifuge tube and attached the top part of the tube onto ITO substrate using epoxy. When epoxy fully dried, (a) for GO/TM electrode sample, dropped cast 20 μ L GO (4 mg/mL) solution to cover whole ITO surface, heated at 60 °C for several minutes until formed thin GO film. When surface cooled down, dipped different volumes of TM solution onto surfaces and dried at 4 °C overnight to obtain GO/TM modified electrode. (b) For the biohybrid/TM electrode sample, pressed biohybrids onto the ITO substrate and dipped the TM solution on top, and still dried at 4 °C overnight. (c) For the Anabaena electrode, dropped cast of 20 μ L cultured Anabaena solution onto the bare ITO electrode or GO coated electrode as described previously and dried at 4 °C for 12 hours.

4.4.4 Photocurrent measurement

Fabricated electrodes in 4.4.3 were used as the working electrode, Ag/AgCl as the reference electrode and carbon cloth as the counter electrode. A home-built system that included a liquid light guide and a \varnothing 5 mm collimator (Olympus BX / IX, ARC: 350-700 nm) to focus light into a diameter of 22 mm was built, a short pass filter with cut-on wavelength 700 nm (FESH0700 - \varnothing 25.0 mm) as well as a long pass filter with cut-on wavelength 550 nm (FEL0550 - \varnothing 1") was used for light irradiation. The power density at 680 nm is determined to be 60 mW/cm² based on the measurements of a light meter (Digi-Sense WD-20250-00). PBS was used as the electrolyte for the photocurrent measurement. The applied potential for all photocurrent measurements was 0.5 V vs Ag/AgCl unless stated otherwise.

Reference

- (1) Huang, J.; Liu, S.; Zhang, C.; Wang, X.; Pu, J.; Ba, F.; Xue, S.; Ye, H.; Zhao, T.; Li, K.; et al. Programmable and Printable Bacillus Subtilis Biofilms as Engineered Living Materials. *Nat. Chem. Biol.* **2019**, *15* (1), 34–41.
- (2) Nguyen, P. Q.; Courchesne, N. M. D.; Duraj-Thatte, A.; Praveschotinunt, P.; Joshi, N. S. Engineered Living Materials: Prospects and Challenges for Using Biological Systems to Direct the Assembly of Smart Materials. *Adv. Mater.* **2018**, *30* (19), 1–34.
- (3) Nudelman, F.; Sommerdijk, N. A. J. M. Biomineralization as an Inspiration for Materials Chemistry. *Angew. Chemie Int. Ed.* **2012**, *51* (27), 6582–6596.
- (4) Liu, S.; Xu, W. Engineered Living Materials-Based Sensing and Actuation . *Frontiers in Sensors* . 2020.

- (5) Sung-Jin, P.; Mattia, G.; Soo, P. K.; Shirley, P.; Valentina, D. S.; L., B. E.; U., L. J.; H., C. P.; Stephanie, D.; K., C. A.; et al. Phototactic Guidance of a Tissue-Engineered Soft-Robotic Ray. *Science* **2016**, *353* (6295), 158–162.
- (6) Gerber, L. C.; Koehler, F. M.; Grass, R. N.; Stark, W. J. Incorporation of Penicillin-Producing Fungi into Living Materials to Provide Chemically Active and Antibiotic-Releasing Surfaces. *Angew. Chemie Int. Ed.* **2012**, *51* (45), 11293–11296.
- (7) Smith, R. S. H.; Bader, C.; Sharma, S.; Kolb, D.; Tang, T.-C.; Hosny, A.; Moser, F.; Weaver, J. C.; Voigt, C. A.; Oxman, N. Hybrid Living Materials: Digital Design and Fabrication of 3D Multimaterial Structures with Programmable Biohybrid Surfaces. *Adv. Funct. Mater.* **2020**, *30* (7), 1907401.
- (8) Moser, F.; Tham, E.; González, L. M.; Lu, T. K.; Voigt, C. A. Light-Controlled, High-Resolution Patterning of Living Engineered Bacteria Onto Textiles, Ceramics, and Plastic. *Adv. Funct. Mater.* **2019**, 29 (30), 1901788.
- (9) Liu, X.; Tang, T.-C.; Tham, E.; Yuk, H.; Lin, S.; Lu, T. K.; Zhao, X. Stretchable Living Materials and Devices with Hydrogel{\text{textendash}}elastomer Hybrids Hosting Programmed Cells. *Proc. Natl. Acad. Sci.* **2017**, *114* (9), 2200–2205.
- (10) Schaffner, M.; Rühs, P. A.; Coulter, F.; Kilcher, S.; Studart, A. R. 3D Printing of Bacteria into Functional Complex Materials. *Sci. Adv.* **2017**, *3* (12).
- (11) Balasubramanian, S.; Yu, K.; Meyer, A. S.; Karana, E.; Aubin-Tam, M.-E. Bioprinting of Regenerative Photosynthetic Living Materials. *Adv. Funct. Mater.* **2021**, *31* (31), 2011162.
- (12) Balasubramanian, S.; Aubin-Tam, M.-E.; Meyer, A. S. 3D Printing for the Fabrication of Biofilm-Based Functional Living Materials. *ACS Synth. Biol.* **2019**, *8* (7), 1564–1567.
- (13) Chen, A. Y.; Zhong, C.; Lu, T. K. Engineering Living Functional Materials. *ACS Synth. Biol.* **2015**, *4* (1), 8–11.
- (14) McBee, R. M.; Lucht, M.; Mukhitov, N.; Richardson, M.; Srinivasan, T.; Meng, D.; Chen, H.; Kaufman, A.; Reitman, M.; Munck, C.; et al. Engineering Living and Regenerative Fungal–Bacterial Biocomposite Structures. *Nat. Mater.* **2021**.
- (15) Dundas, C. M.; Graham, A. J.; Romanovicz, D. K.; Keitz, B. K. Extracellular Electron Transfer by Shewanella Oneidensis Controls Palladium Nanoparticle Phenotype. *ACS Synth. Biol.* **2018**, *7* (12), 2726–2736.
- (16) Hsu, L. (Huan-H.; Deng, P.; Zhang, Y.; Nguyen, H. N.; Jiang, X. Nanostructured Interfaces for Probing and Facilitating Extracellular Electron Transfer. *J. Mater. Chem. B* **2018**, *6* (44), 7144–7158.
- (17) Pedireddy, S.; Jimenez-Sandoval, R.; Ravva, M. K.; Nayak, C.; Anjum, D. H.; Jha, S. N.; Katuri, K. P.; Saikaly, P. E. Harnessing the Extracellular Electron Transfer Capability of Geobacter Sulfurreducens for Ambient Synthesis of Stable Bifunctional Single-Atom Electrocatalyst for Water Splitting. *Adv. Funct. Mater.* **2021**, *31* (22), 2010916.
- (18) Jiang, X.; Hu, J.; Lieber, A. M.; Jackan, C. S.; Biffinger, J. C.; Fitzgerald, L. A.; Ringeisen, B. R.; Lieber, C. M. Nanoparticle Facilitated Extracellular Electron Transfer in Microbial Fuel Cells. *Nano Lett.* 2014, 14 (11), 6737–6742.
- (19) Nakamura, R.; Kai, F.; Okamoto, A.; Newton, G. J.; Hashimoto, K. Self-Constructed

- Electrically Conductive Bacterial Networks. *Angew. Chemie Int. Ed.* **2009**, *48* (3), 508–511.
- (20) Tseng, C.-P.; Silberg, J. J.; Bennett, G. N.; Verduzco, R. 100th Anniversary of Macromolecular Science Viewpoint: Soft Materials for Microbial Bioelectronics. *ACS Macro Lett.* **2020**, *9* (11), 1590–1603.
- (21) TerAvest, M. A.; Ajo-Franklin, C. M. Transforming Exoelectrogens for Biotechnology Using Synthetic Biology. *Biotechnol. Bioeng.* **2016**, *113* (4), 687–697.
- (22) Kumar, A.; Hsu, L. H.-H.; Kavanagh, P.; Barrière, F.; Lens, P. N. L.; Lapinsonnière, L.; Lienhard V, J. H.; Schröder, U.; Jiang, X.; Leech, D. The Ins and Outs of Microorganism–Electrode Electron Transfer Reactions. *Nat. Rev. Chem.* **2017**, *1*, 24.
- (23) Xiao, N.; Wu, R.; Huang, J. J.; Selvaganapathy, P. R. Development of a Xurographically Fabricated Miniaturized Low-Cost, High-Performance Microbial Fuel Cell and Its Application for Sensing Biological Oxygen Demand. Sensors Actuators B Chem. 2019, 127432.
- (24) Webster, D. P.; TerAvest, M. A.; Doud, D. F. R.; Chakravorty, A.; Holmes, E. C.; Radens, C. M.; Sureka, S.; Gralnick, J. A.; Angenent, L. T. An Arsenic-Specific Biosensor with Genetically Engineered Shewanella Oneidensis in a Bioelectrochemical System. *Biosens. Bioelectron.* **2014**, *62*, 320–324.
- (25) Deng, P.; Sheng, W.; Xu, A.; Li, C.; Zhang, Y.; Dai, X.; Vo, R.; Kaplan, D. L.; Hsu, H.-H.; Jiang, X. Bottom-Up Construction of Electrochemically Active Living Filters: From Graphene Oxide Mediated Formation of Bacterial Cables to 3D Assembly of Hierarchical Architectures. *ACS Appl. Bio Mater.* **2020**, *3* (11), 7376–7381.
- (26) Hsu, L. H.-H.; Zhang, Y.; Deng, P.; Dai, X.; Jiang, X. Biosynthetic Electronic Interfaces for Bridging Microbial and Inorganic Electron Transport. *Nano Lett.* **2019**, *19* (12), 8787–8792.
- (27) Xu, W.; Jin, Z.; Pang, X.; Zeng, Y.; Jiang, X.; Lu, Y.; Shen, L. Interaction between Biocompatible Graphene Oxide and Live Shewanella in the Self-Assembled Hydrogel: The Role of Physicochemical Properties. *ACS Appl. Bio Mater.* **2020**, *3* (7), 4263–4272.
- (28) Pei, S.; Cheng, H.-M. The Reduction of Graphene Oxide. *Carbon N. Y.* **2012**, *50* (9), 3210–3228.
- (29) Li, D.; Müller, M. B.; Gilje, S.; Kaner, R. B.; Wallace, G. G. Processable Aqueous Dispersions of Graphene Nanosheets. *Nat. Nanotechnol.* **2008**, *3* (2), 101–105.
- (30) Li, M.; Liu, C.; Xie, Y.; Cao, H.; Zhao, H.; Zhang, Y. The Evolution of Surface Charge on Graphene Oxide during the Reduction and Its Application in Electroanalysis. *Carbon N. Y.* **2014**, *66*, 302–311.
- (31) Moreno-Castilla, C. Adsorption of Organic Molecules from Aqueous Solutions on Carbon Materials. *Carbon N. Y.* **2004**, *42* (1), 83–94.
- (32) Beblawy, S.; Bursac, T.; Paquete, C.; Louro, R.; Clarke, T. A.; Gescher, J. Extracellular Reduction of Solid Electron Acceptors by Shewanella Oneidensis. *Mol. Microbiol.* **2018**, 109 (5), 571–583.
- (33) Zhao, C.; Ding, C.; Lv, M.; Wang, Y.; Jiang, L.; Liu, H. Hydrophilicity Boosted Extracellular Electron Transfer in Shewanella Loihica PV-4. *RSC Adv.* **2016**, *6* (27),

- 22488-22493.
- (34) Ye, Z.; Ellis, M. W.; Nain, A. S.; Behkam, B. Effect of Electrode Sub-Micron Surface Feature Size on Current Generation of Shewanella Oneidensis in Microbial Fuel Cells. *J. Power Sources* **2017**, *347*, 270–276.
- (35) Malvankar, N. S.; Vargas, M.; Nevin, K. P.; Franks, A. E.; Leang, C.; Kim, B.-C.; Inoue, K.; Mester, T.; Covalla, S. F.; Johnson, J. P.; et al. Tunable Metallic-like Conductivity in Microbial Nanowire Networks. *Nat. Nanotechnol.* 2011, 6 (9), 573–579.
- (36) Malvankar, N. S.; Tuominen, M. T.; Lovley, D. R. Biofilm Conductivity Is a Decisive Variable for High-Current-Density Geobacter Sulfurreducens Microbial Fuel Cells. *Energy Environ. Sci.* **2012**, *5* (2), 5790–5797.
- (37) Hsu, L.; Deng, P.; Zhang, Y.; Jiang, X. Core/Shell Bacterial Cables: A One-Dimensional Platform for Probing Microbial Electron Transfer. *Nano Lett.* **2018**, *18* (7), 4606–4610.
- (38) Xu, S.; Barrozo, A.; Tender, L. M.; Krylov, A. I.; El-Naggar, M. Y. Multiheme Cytochrome Mediated Redox Conduction through Shewanella Oneidensis MR-1 Cells. *J. Am. Chem. Soc.* **2018**, *140* (32), 10085–10089.
- (39) Samajdar, R. N.; Manogaran, D.; Yashonath, S.; Bhattacharyya, A. J. Using Porphyrin–Amino Acid Pairs to Model the Electrochemistry of Heme Proteins: Experimental and Theoretical Investigations. *Phys. Chem. Chem. Phys.* **2018**, *20* (15), 10018–10029.
- (40) Ringeisen, B. R.; Henderson, E.; Wu, P. K.; Pietron, J.; Ray, R.; Little, B.; Biffinger, J. C.; Jones-Meehan, J. M. High Power Density from a Miniature Microbial Fuel Cell Using Shewanella Oneidensis DSP10. *Environ. Sci. Technol.* **2006**, *40* (8), 2629–2634.
- (41) Kim, H. J.; Park, H. S.; Hyun, M. S.; Chang, I. S.; Kim, M.; Kim, B. H. A Mediator-Less Microbial Fuel Cell Using a Metal Reducing Bacterium, Shewanella Putrefaciens. *Enzyme Microb. Technol.* **2002**, *30* (2), 145–152.
- (42) Xie, X.; Criddle, C.; Cui, Y. Design and Fabrication of Bioelectrodes for Microbial Bioelectrochemical Systems. *Energy Environ. Sci.* **2015**, 8 (12), 3418–3441.
- (43) Dávila, D.; Esquivel, J. P.; Sabaté, N.; Mas, J. Silicon-Based Microfabricated Microbial Fuel Cell Toxicity Sensor. *Biosens. Bioelectron.* **2011**, *26* (5), 2426–2430.
- (44) Di Lorenzo, M.; Thomson, A. R.; Schneider, K.; Cameron, P. J.; Ieropoulos, I. A Small-Scale Air-Cathode Microbial Fuel Cell for on-Line Monitoring of Water Quality. *Biosens. Bioelectron.* **2014**, *62*, 182–188.
- (45) Weng, Z.; Su, Y.; Wang, D.-W.; Li, F.; Du, J.; Cheng, H.-M. Graphene–Cellulose Paper Flexible Supercapacitors. *Adv. Energy Mater.* **2011**, *1* (5), 917–922.
- (46) Wang, X.; Lu, X.; Liu, B.; Chen, D.; Tong, Y.; Shen, G. Flexible Energy-Storage Devices: Design Consideration and Recent Progress. *Adv. Mater.* **2014**, *26* (28), 4763–4782.
- (47) Fortunati, E.; Kenny, J. M.; Torre, L. 5 Lignocellulosic Materials as Reinforcements in Sustainable Packaging Systems: Processing, Properties, and Applications. In *Woodhead Publishing Series in Composites Science and Engineering*; Verma, D., Fortunati, E., Jain, S., Zhang Biopolymer-Based Materials, and Bioenergy, X. B. T.-B., Eds.; Woodhead Publishing, 2019; pp 87–102.
- (48) Alvarez-Paggi, D.; Hannibal, L.; Castro, M. A.; Oviedo-Rouco, S.; Demicheli, V.; Tórtora,

- V.; Tomasina, F.; Radi, R.; Murgida, D. H. Multifunctional Cytochrome c: Learning New Tricks from an Old Dog. *Chem. Rev.* **2017**, *117* (21), 13382–13460.
- (49) Hasan, K.; Milton, R. D.; Grattieri, M.; Wang, T.; Stephanz, M.; Minteer, S. D. Photobioelectrocatalysis of Intact Chloroplasts for Solar Energy Conversion. *ACS Catal.* **2017**, 7 (4), 2257–2265.
- (50) Vo, R.; Hsu, H.-H.; Jiang, X. Hydrogel Facilitated Bioelectronic Integration. *Biomater. Sci.* **2021**, 9, 23–27.
- (51) Wu, S.; Kim, E.; Li, J.; Bentley, W. E.; Shi, X.-W.; Payne, G. F. Catechol-Based Capacitor for Redox-Linked Bioelectronics. *ACS Appl. Electron. Mater.* **2019**, *1* (8), 1337–1347.
- (52) Lennicke, C.; Rahn, J.; Lichtenfels, R.; Wessjohann, L. A.; Seliger, B. Hydrogen Peroxide Production, Fate and Role in Redox Signaling of Tumor Cells. *Cell Commun. Signal.* **2015**, *13* (1), 39.
- (53) Kato, Y.; Nagao, R.; Noguchi, T. Redox Potential of the Terminal Quinone Electron Acceptor QB in Photosystem II Reveals the Mechanism of Electron Transfer Regulation. *Proc. Natl. Acad. Sci.* **2016**, *113* (3), 620–625.
- (54) Mullineaux, C. W. Co-Existence of Photosynthetic and Respiratory Activities in Cyanobacterial Thylakoid Membranes. *Biochim. Biophys. Acta Bioenerg.* **2014**, *1837* (4), 503–511.
- (55) Liu, L. N. Distribution and Dynamics of Electron Transport Complexes in Cyanobacterial Thylakoid Membranes. *Biochim. Biophys. Acta Bioenerg.* **2016**, *1857* (3), 256–265.
- (56) Beveridge, T. J.; Chang, I. S.; Kim, B. H.; Kim, S.; Culley, D. E.; Reed, S. B.; Margaret, F.; Saffarini, D. A.; Hill, E. A.; Shi, L.; et al. Electrically Conductive Bacterial Nanowires Produced by Shewanella Oneidensis Strain MR-1 and Other Microorganisms. *Proc. Natl. Acad. Sci.* **2009**, *106* (23), 9535–9535.